International Geology Review
Publication details, including instructions for authors and subscription information:
http://www.tandfonline.com/loi/tigr20

Dating thin zircon rims by NanoSIMS: the Fengtien nephrite (Taiwan) is the youngest jade on Earth

Tzen-Fu Yui[a], Tadashi Usuki[a], Chun-Yen Chen[a], Akizumi Ishida[b], Yuji Sano[b], Kenshi Suga[a], Yoshiyuki Iizuka[a] & Chih-Tung Chen[a]

[a] Institute of Earth Sciences, Academia Sinica , Taipei, 11529, Taiwan, ROC

[b] Atmosphere and Ocean Research Institute, The University of Tokyo , Kashiwa, Chiba, 2778564, Japan

Published online: 31 Oct 2014.

International Geology Review, 2014
Vol. 56, No. 16, 1932–1944, http://dx.doi.org/10.1080/00206814.2014.972994

Taylor & Francis
Taylor & Francis Group

Dating thin zircon rims by NanoSIMS: the Fengtien nephrite (Taiwan) is the youngest jade on Earth

Tzen-Fu Yui[a]*, Tadashi Usuki[a], Chun-Yen Chen[a], Akizumi Ishida[b], Yuji Sano[b], Kenshi Suga[a], Yoshiyuki Iizuka[a] and Chih-Tung Chen[a]

[a]*Institute of Earth Sciences, Academia Sinica, Taipei, 11529, Taiwan, ROC;* [b]*Atmosphere and Ocean Research Institute, The University of Tokyo, Kashiwa, Chiba, 2778564, Japan*

(*Received 12 August 2014; accepted 1 October 2014*)

Nephrite in the Fengtien area of the eastern part of the Central Mountain Range, Taiwan, is associated with antigorite-serpentinite within the Yuli belt, a late Cenozoic subduction–accretionary complex related to the eastward subduction of the South China Sea plate forming the Luzon arc. Diopsidite and clinozoisite rock are two other metasomatic components accompanying nephrite between serpentinites and the greenschist-facies country rock (carbonaceous material-)quartz-mica schist. Detrital zircons were separated from one clinozoisite rock sample, formed through metasomatic replacement after mica-quartz schist at temperatures of 320–420°C or slightly lower, which is lower than the metamorphic temperature conditions of the Yuli belt. Most of the detrital zircons have thin zircon rims less than 15–20 μm wide. These zircon rims, considered as newly formed during metasomatism leading to nephrite/diopsidite/clinozoisite rock formation, were dated by a high lateral resolution secondary ion mass spectrometer (CAMECA NanoSIMS NS50). The resulting $^{238}U/^{206}Pb$-$^{204}Pb/^{206}Pb$ inverse isochron gave an age of 3.3 ± 1.7 Ma. The collision of the Eurasian continental margin with the Luzon arc has been suggested to have begun at ca. 6.5 Ma in the Taiwan area. The nephrite formation processes therefore clearly post-dated South China Sea plate subduction. The present date, substantiated by the metamorphic and metasomatic temperature information, demonstrates that the fluid–rock interaction forming Fengtien nephrite would have taken place during a Barrovian-type metamorphic overprint resulting from arc-continent collision, leading to the exhumation of the Yuli belt. This conclusion on nephrite formation with regard to regional tectonics can serve as a working model for future studies on other nephrite deposits with similar occurrences, mostly embedded within Mesozoic or older subduction-accretionary complexes. The Fengtien nephrite deposit is therefore the youngest one of its kind exposed on Earth's surface.

Keywords: nephrite; zircon; U-Pb dating; NanoSIMS; Taiwan

1. Introduction

There are two kinds of jade stones associated with serpentinites in mountain belts at convergent plate boundaries. One is nephrite jade, enriched in Ca and Mg, and the other is jadeite jade (or jadeitite), enriched in Na and Al. Both kinds of jade result from metasomatic reactions between serpentinites and country rocks/tectonic blocks taking place, presumably, within convergent environments (Harlow and Sorensen 2005; Harlow *et al*. 2007, 2014). The age of these jade stones could provide useful time constraints for deciphering the evolution of the subduction system in question (e.g. Yui *et al*. 2010; Flores *et al*. 2013; Stern *et al*. 2013). In the past few years, dating jadeitite through *in situ* zircon U-Pb isotope analysis has been thriving (Tsujimori and Harlow 2012 and references therein), although the results have also led to debates regarding whether zircons from jadeitite are inherited, (partially) recrystallized, or newly formed in nature (e.g. Bulle *et al*. 2010; Yui *et al*. 2013). In contrast, little age dating work has been conducted for nephrite jade associated with serpentinite. Lanphere and Hockley (1976) successfully applied the ^{40}Ar-^{39}Ar method for age determination of nephrite from the great serpentinite belt of New South Wales, Australia. The method, however, has not been widely applied to other occurrences, probably due to the low K content and the possible presence of excess Ar in nephrite resulting from metasomatism. Adams *et al*. (2007) reported Rb-Sr isotope data for New Zealand nephrite. However, the meaning of the regression ages is not certain. Although zircon U-Pb dating results should be more robust than K-Ar or Rb-Sr dating of nephrite, it is rarely reported for serpentinite-associated nephrite jade. In this study, instead of trying to retrieve zircons from nephrite, as an alternative, detrital zircons were separated from one sample of clinozoisite rock from Fengtien, Taiwan, considered to have formed through the same metasomatic processes responsible for producing nephrite (Yui and Wang Lee 1980). Fengtien nephrite is the raw material for the famous 'Taiwan Jade' jewellery and artefacts produced in the 1970s. The high-quality nephritic stones are massive in appearance and green to dark green in colour and are highly valued by the local

*Corresponding author. Email: tfyui@earth.sinica.edu.tw

people. We found that a newly formed metasomatic zircon overgrowth, <15–20 μm thick, is always present along zircon cracks and around zircon grains. This thin overgrowth has been dated by NanoSIMS, and the resulting age is inferred as the time of nephrite formation. The implications of this date in terms of nephrite formation within the framework of regional tectonics will be discussed.

2. Geological background and sampling

Taiwan is located at the junction of the Eurasia and the Philippine Sea plates (Figure 1a). The formation of Taiwan island is due to the still ongoing collision/accretion of the Luzon arc with the eastern margin of South China, starting from the Mio–Pliocene (Ho 1986). It is generally considered that the eastern margin of South China in the Taiwan region was active with westward subduction of the Palaeo-Pacific plate during the Late Cretaceous. Westward subduction stopped during the early Eocene and the margin began to rift. With continuous rifting, the South China Sea plate formed during the Oligocene, which then subducted eastward beneath the Philippine Sea plate forming the Luzon arc in the middle Miocene. The arc subsequently collided with and accreted to the South China margin during the late Cenozoic, forming the island of Taiwan (e.g. Ho 1986). In this tectonic framework, Taiwan is divided into two parts by the Longitudinal Valley (i.e. geologic Unit VI in Figure 1a). East of the Valley is the Coastal Range (Unit V), which belongs to the Luzon arc. West of the Valley are geologic Units I–IV, belonging to South China of the Eurasia plate. Unit I is the eastern flank of the Central Range, including subunits of Tailuko belt (Ia) (pre-Cenozoic basement) and Yuli belt (Ib); Unit II, the western flank of the Central Range (Tertiary slate and argillite); Unit III, the western foothill; and Unit IV, the coastal plain.

The Yuli belt (subunit Ib) is marked by a monotonous lithology, composed of greenschist-facies (carbonaceous material-)quartz-mica schist (commonly called black schist) with subordinate metabasite/greenschist, metamorphosed ophiolitic rocks and a few high-pressure (HP) rocks. The HP rocks, including glaucophane schist in the Juisui area and omphacite-zoisite metabasite in the Wanjung area (Figure 1a), are always associated with serpentinite and occur as tectonic blocks on top of other Yuli rocks (Yang and Wang 1985; Lin 1999). Their peak metamorphic conditions were estimated at ~550°C and 10–12 kbar (Beyssac *et al*. 2008). Eclogites have not been reported. The belt was previously regarded as a Cretaceous subduction-accretion complex (see Yui *et al*. 2009, 2012). However, recent finding of Cenozoic detrital zircons demonstrates that most of the belt is late Cenozoic in age (Lo *et al*. 2012; Chen *et al*. 2013; Yui 2013). Its exact boundary with other tectonic units is yet to be defined. Nephrite jade, in association with antigorite-serpentinite, occurs near Fengtien village in this belt (Figure 1). At Fengtien, serpentinites crop out as layers or lenses, 5–50 m thick and 100–3000 m long, intercalated with mica-quartz schist. The contacts between

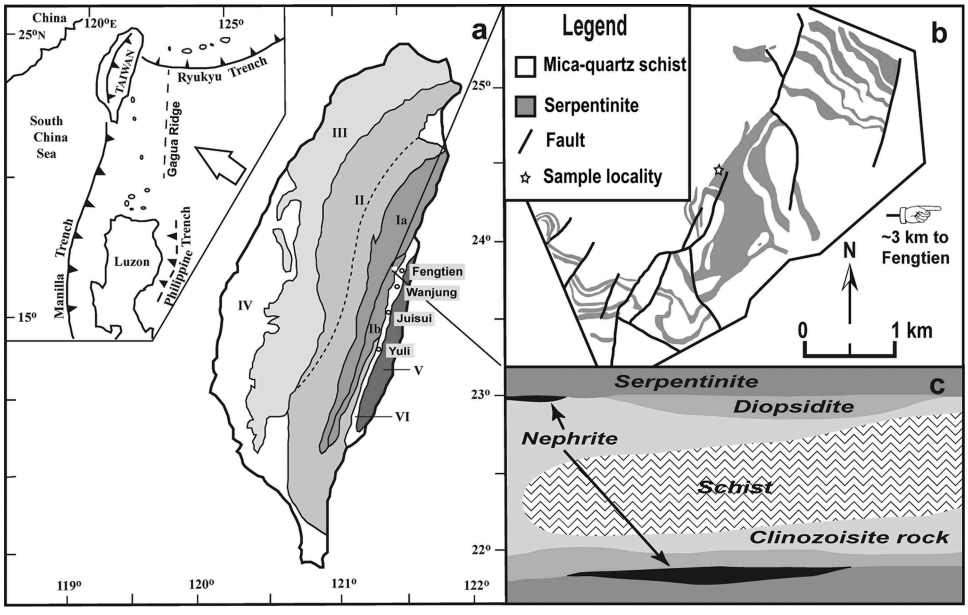

Figure 1. (a) Major tectonic units of Taiwan (Ho 1986). I: the eastern flank of the Central Range, Ia. Tailuko belt, Ib. Yuli belt; II: the western flank of the Central Range (Tertiary slate and argillite); III: the western foothill; IV: the coastal plain; V: the Coastal Range; VI: the Longitudinal Valley. Serpentinites occur in the Yuli belt near the villages of Fengtien, Wanjung, Juisui, and Yuli. (b) Geological map of the Fengtien serpentinite area (after Tan *et al*. 1978). (c) Schematic diagram (not in scale) showing the common lithologic relation between serpentinite, nephrite, diopsidite, clinozoisite rock, and schist observed in mining adits.

serpentinites and schists are generally concordant, but discordant ones due to late-stage tectonic movement were also observed locally. The foliation of the schist strikes mainly E–W or ENE with a 20° to 30° dip towards the north (Tan *et al*. 1978). Nephrite mainly occurs sporadically as lenses at the contact between serpentinites and mica-quartz schist through metasomatic reactions (Yui and Wang Lee 1980). Besides nephrite, other metasomatic rocks such as diopsidite and clinozoisite rock are also present. When all rock types are present in one outcrop, the common lithologic sequence is serpentinite-nephrite-diopsidite-clinozoisite rock-schist (Figure 1c). Occasionally, nephrite occurs between diopsidite and clinozoisite rock. Repetition of the sequence, although rare, has also been observed. The thickness of this Ca-Mg-metasomatic sequence varies from 0.1 to 2 m. While nephrite was formed after serpentinite or ultramafic rocks, clinozoisite rock replacing schist is evidenced by gradational mineralogical changes (Tan *et al*. 1978; Yui and Wang Lee 1980). The metasomatic processes responsible for the formation of diopsidite, however, are not yet clear. The contact relation between the various metasomatic zones is temporally complicated and varies from place to place. As a whole, these metasomatic zones formed more or less contemporaneously (Tan *et al*. 1978). Late-stage metasomatic minerals, including grossular, diopside, zoisite, tremolite, quartz, chlorite, and calcite in fissure cracks are common. Temperatures for serpentinization and associated metasomatic processes were estimated in the range of 320–420°C based on phase relations and stable isotope fractionations between vein minerals (Yui *et al*. 1988, 1990).

The clinozoisite rock sample, SCY-4, in this study was collected from an abandoned mining adit in the Fengtien area (Figure 1b), where nephrite occurs at the hanging wall of a serpentinite layer. Diopsidite is not present at this locality, and clinozoisite rock therefore occurs between serpentinite/nephrite and mica-quartz schist. Two more samples were also collected to examine chemical variations of chlorite, as well as the Raman spectrum of carbonaceous material for temperature estimation. Sample SCY-5 is a partially metasomatized schist, comprising mica-quartz-rich layers and clinozoisite-chlorite-rich layers, whereas sample SCY-6 is a typical mica-quartz schist from the area.

3. Analytical methods

Quantitative chemical analyses of minerals in the present study were made using a JEOL electron microprobe (JEOL, Tokyo, Japan) equipped with wave-length dispersive spectrometers at the Institute of Earth Sciences, Academia Sinica. Secondary- and back-scattered electron images were used to guide the analysis on target positions of minerals. A 2 μm defocused beam was used at an acceleration voltage of 15 kV with a beam current of 10 nA.

Raman spectroscopy of carbonaceous material (RSCM) was obtained using a Renishaw inVia microspectrometer (Renishaw plc., Wootton-under-Edge, UK) equipped with a 514 nm argon laser housed in Tatung University, Taipei, Taiwan. The laser was focused on the thin section surface using a DMLM Leica microscope (Leica Microsystems GmbH, Wetzlar, Germany) with a 50× objective, and the laser power at the sample surface was set at around 1 mW. The signal was filtered by edge filters and finally dispersed using a 1800 gr/mm grating to be analysed by a Peltier cooled CCD detector. Analytical and fitting procedures described by Beyssac *et al*. (2002) were strictly followed to avoid analytical pitfalls. For each sample, more than 10 spectra were measured and processed using the software Peakfit following Beyssac *et al*. (2003).

Zircons from clinozoisite rock sample SCY-4, concentrated by standard heavy mineral separation processes and hand picking for final purity, were mounted in an epoxy (Araldite502) disc with a 10 mm diameter and a 2 mm thickness. All grains were imaged with transmitted light and reflected light under a petrographic microscope. Cathodoluminescence (CL) images and secondary electron micrographs (SEM) were taken with a JEOL 5600 SEM to identify internal and surface texture. A LABRAM HR confocal micro-Raman spectrometer (Horiba Jobin Yvon, Paris, France) equipped with a Ar^{+} laser with 514 nm excitation, housed in the Institute of Earth Sciences, Academia Sinica, was employed to examine crystal structure of the newly formed zircon rims. The laser beam size was about 2–5 μm, and the laser power on the sample surface was about 15 mW.

In situ U-Pb dating analyses on zircon rims were performed with an ion microprobe (NanoSIMS NS50, Ametek, Inc., Paris, France) at the Atmosphere and Ocean Research Institute of the University of Tokyo. The zircon disc was cleaned with ethanol and pure water and coated with gold to dissipate any charging during the SIMS analysis. Zircon was sputtered by a ~5 nA mass filtered O^{-} primary beam with a spot size of ~10 μm on the zircon surface. Before analysis, zircon was pre-sputtered for 5 min to remove the surface Au coating and any possible surface contaminants. During this pre-sputtering, ion beams were tuned contemporaneously. Secondary ions of $^{204}Pb^{+}$, $^{206}Pb^{+}$, $^{238}U^{16}O^{+}$, and $^{238}U^{16}O_2^{+}$ were then measured simultaneously for 500 s through the multi-collector system. A mass resolution of about 4000 at 10% peak height and with a flat peak top was attained.

The $^{206}Pb/^{238}U$ ratio of sample zircons was estimated by the following empirical equation:

$$\left(^{206}Pb/^{238}U\right) = \left(^{206}Pb^{*}/^{238}U\right)_{AS3} \times \left(^{206}Pb^{+}/^{238}UO^{+}\right)/[a \times \left(UO_2^{+}/UO^{+}\right)^2 + b],$$

where Pb* is radiogenic lead and constants a and b were estimated, using the York Method (York 1968), by repeated measurements at different disc positions along the secondary ion extraction direction on standard zircons (AS3) with a recommended age of 1099.1 ± 0.5 Ma from the gabbroic anorthosite of the Duluth Complex, northeastern Minnesota (Paces and Miller 1993; Schmitz *et al.* 2003). Due to the young age of sample zircon rims, common lead correction is difficult. The age of these zircon rims was then derived by a $^{238}U/^{206}Pb$–$^{204}Pb/^{206}Pb$ isochron plot under the assumption that all rims formed at the same time. Uncertainty of the age was estimated by error propagation of the uncertainty of the $^{206}Pb/^{238}U$ and $^{204}Pb/^{206}Pb$ ratios. More details on the dating protocol are given in Takahata *et al.* (2008).

4. Results

4.1. Sample description and temperature estimate

The clinozoisite rock sample SCY-4 is mainly composed of clinozoisite (75 vol%) and chlorite (20 vol%), with minor (5 vol%) quartz, allanite, titanite, apatite, and zircon (Figure 2a). The mineral grain size is about 0.05–0.25 mm. Clinozoisite shows a weak preferred orientation inherited from mica-quartz schist. Quartz is observed as inclusions in clinozoisite but not in the matrix. Late-stage quartz and actinolite veinlets are common. Representative chemical compositions of minerals are given in Table 1. Clinozoisite is commonly richer in Fe at core (average Ps = 0.16) than at rim (average Ps = 0.11). Some cores can actually be classified as epidote. Chlorite is clinochlore (Figure 3).

Sample SCY-5 is a partially metasomatized mica-quartz schist with local enrichment of clinozoisite + chlorite along cleavages. The modal composition therefore varies from mica-quartz-rich layers (Figure 2d) to clinozoisite-chlorite-rich layers (Figure 2c). In either case, quartz is present in the matrix. Clinozoisite in the latter layers shows similar chemical composition to that in the clinozoisite rock sample SCY-4 mentioned earlier (Table 1). In contrast, chlorites in both kinds of zones vary considerably in Fe and Mg contents and are either clinochlore or chamosite (Figure 3). A few chlorites, mostly in clinozoisite-chlorite-rich layers, in this sample are chemically similar to chlorite in the clinozoisite rock sample SCY-4 (Figure 3). Obviously, chlorites in this sample are not in chemical equilibrium, in accord with the idea that they

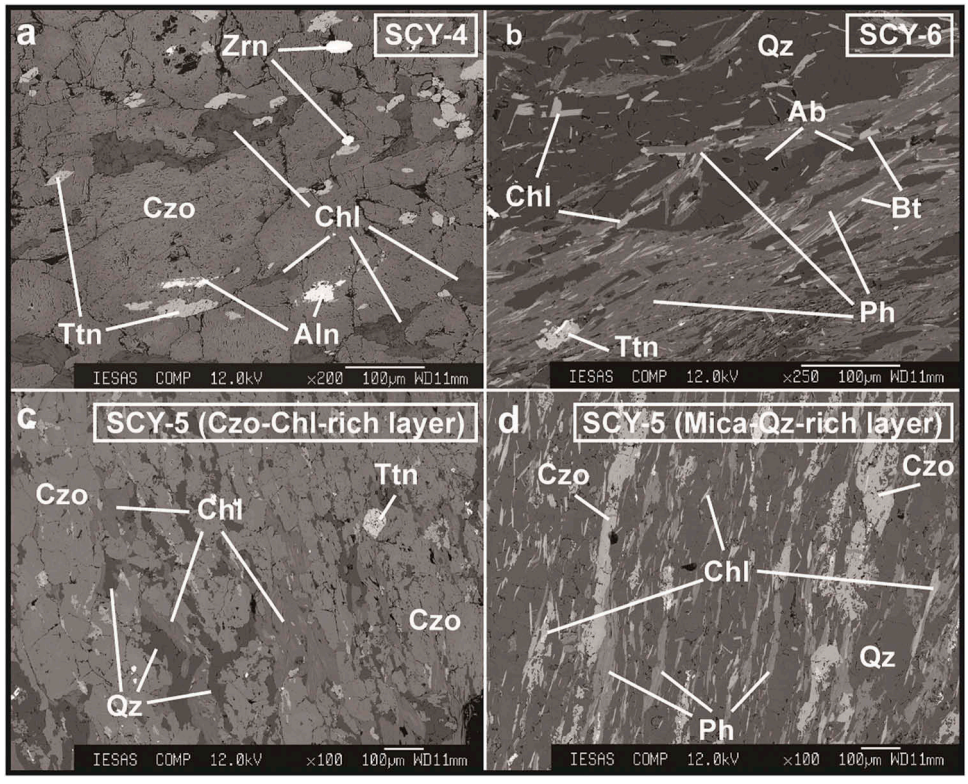

Figure 2. Back-scattered electron images of (a) SCY-4, clinozoisite rock; (b) SCY-6, mica-quartz schist; (c) SCY-5, clinozoisite-chlorite-rich layer of partially metasomatized mica-quartz schist; and (d) SCY-5, mica-quartz-rich layer of partially metasomatized mica-quartz schist. Mineral abbreviations are: Ab, albite; Aln, allanite; Bt, biotite; Chl, chlorite; Czo, clinozoisite; Ph, phengite; Qz, quartz; Ttn, titanite; and Zrn, zircon. White scale bars are 100 μm.

Table 1. Representative chemical composition of minerals.

	SCY-4			SCY-5					SCY-6			
	Clinozoisite			Clinozoisite		Chlorite						
	Core	Rim	Chlorite	Core	Rim	With qtz[c]	With czo[d]	Phengite	Chlorite	Biotite	Phengite	Albite
SiO_2	38.28	38.49	28.59	38.24	39.05	25.62	26.63	48.90	24.69	37.09	48.77	68.92
TiO_2	0.04	0.12	0.00	0.17	0.07	0.01	0.04	0.12	0.07	1.93	0.16	0.00
Al_2O_3	28.08	29.43	17.97	28.64	28.95	20.78	21.57	29.36	20.91	18.26	28.18	19.69
FeO[a]	–	–	18.23	–	–	25.11	18.99	3.17	30.13	22.26	3.50	0.10
Fe_2O_3[b]	8.53	5.71	–	7.64	5.48	–	–	–	–	–	–	–
MnO[a]	–	–	0.28	–	–	0.48	0.40	0.05	0.69	0.37	0.00	0.07
Mn_2O_3[b]	0.30	0.16	–	0.09	0.21	–	–	–	–	–	–	–
MgO	0.04	0.04	20.87	0.05	0.02	14.14	18.72	2.48	10.77	7.38	2.24	0.00
CaO	23.31	23.94	0.04	23.66	24.68	0.07	0.09	0.06	0.00	0.03	0.00	0.01
Na_2O	0.00	0.00	0.00	0.00	0.00	0.07	0.02	0.12	0.03	0.05	0.19	12.04
K_2O	0.01	0.00	0.01	0.00	0.00	0.00	0.00	10.21	0.07	8.10	9.63	0.08
P_2O_5	0.00	0.00	0.01	–	–	–	–	–	–	–	–	–
Total	98.60	97.90	86.00	98.49	98.46	86.28	86.46	94.46	87.36	95.46	92.67	100.92
	12.5(O)	12.5(O)	28(O)	12.5(O)	12.5(O)	28(O)	28(O)	22(O)	28(O)	22(O)	22(O)	8(O)
Si	2.969	2.980	5.903	2.960	3.009	5.492	5.495	6.601	5.386	5.646	6.698	2.986
Ti	0.002	0.007	0.000	0.010	0.004	0.002	0.006	0.012	0.011	0.221	0.017	0.000
Al	2.567	2.685	4.372	2.613	2.629	5.250	5.245	4.671	5.376	3.276	4.561	1.006
Fe^{2+}	–	–	3.147	–	–	4.501	3.277	0.358	5.496	2.833	0.402	0.004
Fe^{3+}	0.498	0.333	–	0.445	0.318	–	–	–	–	–	–	–
Mn^{2+}	–	–	0.050	–	–	0.087	0.070	0.006	0.127	0.048	0.000	0.003
Mn^{3+}	0.018	0.009	–	0.005	0.014	–	–	–	–	–	–	–
Mg	0.005	0.005	6.424	0.006	0.002	4.519	5.759	0.499	3.503	1.675	0.459	0.000
Ca	1.937	1.986	0.009	1.962	2.038	0.016	0.020	0.009	0.000	0.004	0.000	0.000
Na	0.000	0.000	0.000	0.000	0.000	0.000	0.008	0.031	0.013	0.014	0.050	1.012
K	0.001	0.000	0.003	0.000	0.000	0.000	0.000	1.758	0.021	1.573	1.687	0.004
P	0.000	0.000	0.002	–	–	–	–	–	–	–	–	–
Total	7.997	8.005	19.910	8.001	8.014	19.867	19.880	13.945	19.933	15.290	13.874	5.015
Mg/(Mg+Fe)			0.671			0.501	0.673		0.389			
Ps	0.16	0.11		0.15	0.11							

Notes: [a]Total Fe as FeO or total Mn as MnO.
[b]Total Fe as Fe_2O_3 or total Mn as Mn_2O_3.
[c]Chlorite within mica-quartz-rich layer.
[d]Chlorite within clinozoisite-chlorite-rich layer.

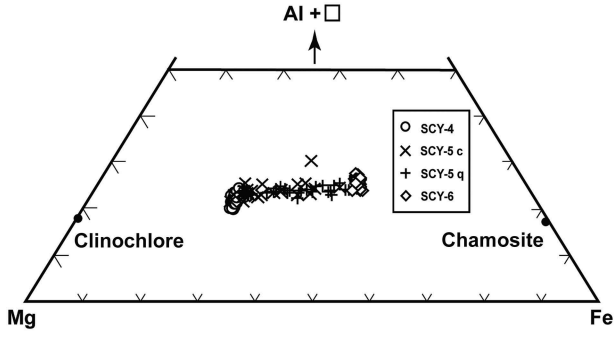

Figure 3. Al+□(octahedral vacancy)-Mg-Fe plot for chlorite after Zane *et al*. (1998). Chlorites in sample SCY-4 are clinochlore; in sample SCY-6 are chamosite; and in sample SCY-5 are either clinochlore or chamosite.

might have formed during the retrograde cooling stage discussed below (see Section 5.1).

Sample SCY-6 is a mica-quartz schist, consisting of quartz (45 vol%), phengite (25 vol%), albite (10 vol%), chlorite (10 vol%), biotite (5 vol%), and minor (~5 vol%) titanite, carbonates, pyrite, apatite, zircon, and carbonaceous material (Figure 2b). Representative chemical analyses for chlorite, biotite, phengite, and albite are given in Table 1. Chlorite is chamosite and is high in Fe content compared with chlorite in clinozoisite rock sample SCY-4 and partially metasomatized mica-quartz schist sample SCY-5 (Figure 3). Chemical variation of chlorite from these rocks clearly demonstrates the Mg-metasomatic effect on samples SCY-4 and 5.

Temperature estimation for the metasomatic processes forming the clinozoisite rock was done following the chlorite thermometry given by Lanari *et al*. (2014). Assuming total Fe as Fe^{2+}, 44 chemical analyses of chlorite in sample SCY-4 gave a temperature range of 153–276°C (with an average of 206 ± 34(1σ)°C) or 172–302°C (with an average of 228 ± 35°C) if P = 3 or 5 kbar,

respectively (see Supplementary Table S1 at http://dx.doi.org/10.1080/00206814.2014.972994); 50 chemical analyses on chlorite in sample SCY-5 gave an estimated temperature range of 268–436°C (with an average of 355 ± 48°C) at 3 kbar or 293–468°C (with an average of 383 ± 51°C) at 5 kbar (see Supplementary Tables S2 and S3); and 27 chemical analyses on chlorite in sample SCY-6 gave an estimated temperature range of 289–454°C (with an average of 358 ± 50°C) at 3 kbar or 314–487°C (with an average of 387 ± 53°C) at 5 kbar (see Supplementary Table S4). The temperature estimates from SCY-4 chlorites are much lower than those from SCY-5 and SCY-6 chlorites, the latter two are comparable. This would be attributed to the constraint that the thermometry was based on the chlorite + quartz + water equilibrium (Lanari *et al*. 2014), and quartz, although observed as inclusions in SCY-4 clinozoisite indicating its presence at least during the early stage of metasomatism, does not occur in SCY-4 rock matrix. Furthermore, the maximum temperature for the chlorite thermometry calibrated by Lanari *et al*. (2014) is 400°C. The calculated temperatures higher than this limit for samples SCY-5 and SCY-6 would be less reliable. Nonetheless, the temperature ranges derived from samples SCY-5 and SCY-6 are in agreement with (or slightly lower than) the previous metasomatic temperature estimates of 320–420°C based on phase diagram and stable isotope fractionations between fissure-filling minerals (Yui *et al*. 1988, 1990).

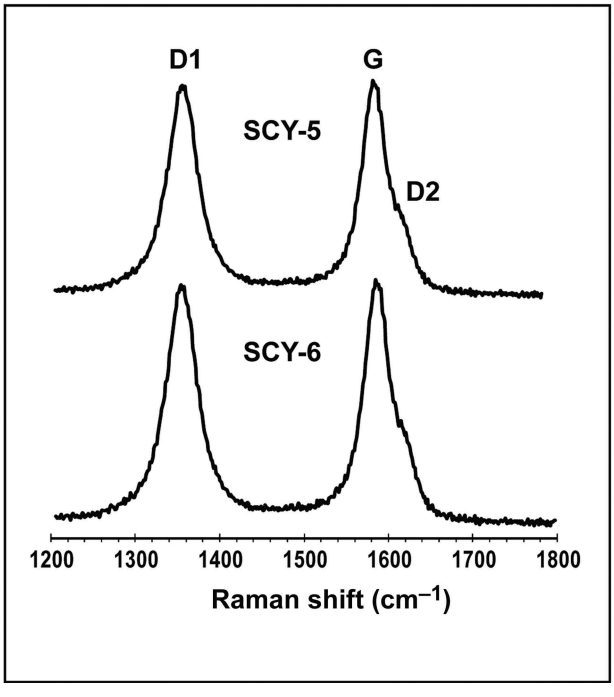

Figure 4. Representative Raman spectrum of carbonaceous material from samples SCY-5 and SCY-6, showing G, D1, and D2 peaks.

Table 2. RSCM temperature estimates.

Sample	Number of analysis	R2[a]	1σ	RSCM-T (°C)	1σ (°C)
SCY-5	12	0.48	0.02	429	8
SCY-6	16	0.52	0.01	408	5

Note: [a]R2 (area ratio) = D1/(G + D1 + D2) (see Figure 4 and Beyssac *et al*. 2002).

Raman spectroscopic analyses on carbonaceous material were carried out for samples SCY-5 and SCY-6. Representative Raman spectra are given in Figure 4, showing similar spectral patterns with G, D1, and D2 peaks for carbonaceous material in both the samples. The resulting temperature estimate is 429°C for sample SCY-5 and 408°C for sample SCY-6 (Table 2). Given that the uncertainty of this RSCM thermometry was suggested to be ±50°C (Beyssac *et al*. 2002), these two results are comparable. These RSCM temperature estimates, 410–430°C, are slightly higher than, although overlap with, the results from the chlorite thermometry. The difference may be inherited from the two different thermometers. Alternatively, or more likely, RSCM, being more robust, recorded metamorphic peak temperature, while chlorite chemistry recorded subsequent metasomatic temperature.

4.2. *CL image and Raman spectrum of zircon*

Representative CL images of zircons from sample SCY-4 are given in Figure 5a–g. Zircons are usually prismatic and subhedral to anhedral in form, demonstrating their detrital nature. The grain size ranges from 60 × 100 to 100 × 200 μm. Most zircons show typical oscillatory zoning, although complicated patchy texture is also present. It is noted that almost all zircons have a bright and featureless thin overgrowth under CL, with a thickness less than ~15–20 μm. Such newly formed zircon was also observed along zircon cracks (Figure 5a, c, d, and g). These newly formed zircon overgrowth features, however, were rarely observed during detrital zircon studies for rocks, similar to sample SCY-6, from both the Tailuko and the Yuli belts of Taiwan (see Figure 4 in Yui *et al*. 2012). These zircon overgrowths are therefore regarded to have formed during the metasomatic processes forming clinozoisite rock and nephrite-diopsidite as well. Raman spectra of these newly formed zircons (not shown) do not show any difference from those of the zircon cores, which are mostly of magmatic origin (Yui 2013). The crystallinity of zircon overgrowths and zircon cores is comparable despite their different formation temperatures.

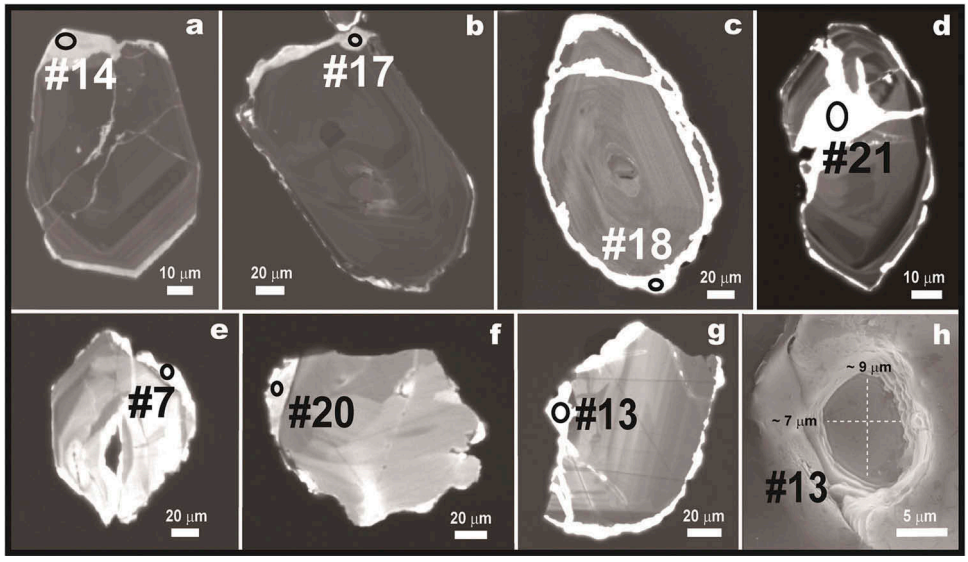

Figure 5. (a)–(g) CL images of zircons from sample SCY-4 showing that the detrital zircons with oscillatory zoning are rimed or cut by bright and featureless newly formed zircon. (h) SEM image of zircon surface showing ion beam sputtering pit after analysis #13.

4.3. U-Pb dating results

To check the dating protocols used in this study, zircons from the Yuantoushan metagranite (sample T-8) in the northern part of the Tailuko belt were employed as a test. Zircons from this metagranite body were previously analysed by the thermal ionization mass spectrometry method giving an age of 86 ± 1 Ma (Jahn *et al*. 1986) or 87 ± 1 Ma (Yui *et al*. 1996) and were also dated by the sensitive high-resolution ion microprobe-reverse geometry (SHRIMP-RG) at the Stanford – US Geological Survey Mass Analysis Center, giving an age of 88 ± 1 Ma (unpublished data, see Supplementary Figure S1 at http://dx.doi.org/10.1080/00206814.2014.972994). These results demonstrate that zircons from this metagranite are homogeneous in age. The results of the Yuantoushan zircons analysed by the present protocols are given in the Supplementary Table S5. In the $^{238}U/^{206}Pb$–$^{204}Pb/^{206}Pb$ plot (Supplementary Figure S1), 10 analyses yielded a regression age of 87 ± 8 Ma (95% confidence limit, mean square weighted deviation (MSWD) = 2.6) and a calculated initial $^{206}Pb/^{204}Pb$ ratio of 18.3 ± 5.3. Although the precision is not as good as for other methods, which is not unexpected, the resulting age is comparable with the previous dates.

At the beginning of analysing zircon rims from sample SCY-4, it was found that both Pb and U contents of these newly formed zircon overgrowths are very low. To avoid possible contaminations from epoxy resin, analyses were therefore restrained to those overgrowths thick enough to accommodate the ion beam size, which is about 10 μm in diameter (Figure 5h). Since most of the overgrowths are thinner than ~10 μm, only seven spot analyses were successfully retrieved. The CL images of these seven zircon grains, as well as a representative SEM photo of the ion beam sputtering pit on zircon analysis #13, are shown in Figure 5. SEM images of other six zircons showing ion beam sputtering pits are given in Supplementary Figure S2. The U-Pb isotope analytical results are given in Table 3 and shown in the $^{238}U/^{206}Pb$–$^{204}Pb/^{206}Pb$ isochron plot (Figure 6). Among the seven analyses, five spots (#13, #17, #18, #20, and #21) yielded results forming an isochron with an age of 3.3 ± 1.7 Ma (95% confidence limit, MSWD = 2.1). The calculated initial $^{206}Pb/^{204}Pb$ ratio of 24.6 ± 8.1 is comparable with the theoretical value of 18.65 (Stacey and Kramers 1975) within error. The other two analyses (#7 and #14) show higher $^{204}Pb/^{206}Pb$ ratios, probably due to the presence of a high common lead component. The regression age obtained is interpreted as the time of metasomatic processes between serpentinite and mica-quartz schist, forming clinozoisite rock, diopsidite, and nephrite.

Table 3. Zircon U-Pb dating results.

	$^{204}Pb/^{206}Pb$	Err (abs, 2σ)	$^{206}Pb/^{238}U$	Err (abs, 2σ)
#7	0.1222	0.0196	0.1578	0.0170
#13	0.0259	0.0101	0.0012	0.0002
#14	0.9015	0.2177	0.0224	0.0055
#17	0.0146	0.0158	0.0010	0.0001
#18	0.0394	0.0237	0.4959	0.1392
#20	0.0454	0.0104	8.0772	4.4084
#21	0.0160	0.0212	0.0108	0.0018

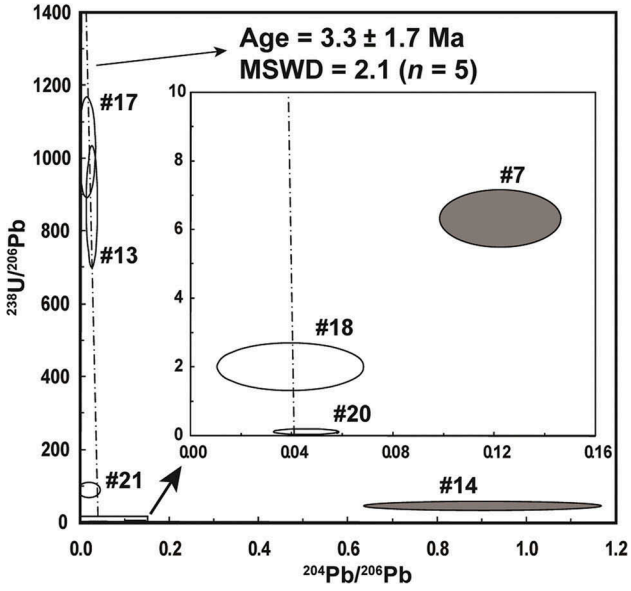

Figure 6. $^{238}U/^{206}Pb$–$^{204}Pb/^{206}Pb$ plot for zircon analyses in this study. Grey circles are analyses excluded from age regression.

5. Discussion

5.1. Tectonic setting for the formation of Fengtien nephrite

The Yuli belt is a late Cenozoic subduction-accretionary complex formed by subduction of the South China Sea plate to form the Luzon arc. The subduction began not later than middle Miocene, as evidenced by the oldest (~16 Ma) arc volcanic rock in northern Luzon arc (i.e. the Coastal Range of Taiwan) (Yang *et al*. 1995). This subduction in the Taiwan region ceased at about 6.5 Ma (Lin *et al*. 2003) when the Luzon arc collided with and accreted to the Eurasia continental margin leading to uplift of the continental margin forming Taiwan Island, although the subduction is now still going on along the Manila Trench south of ~22.5°N (inset of Figure 1a) (Tsai 1986). The age of the youngest detrital zircon grain in sample SCY-4 is 26 Ma (Yui 2013) (see Supplementary Figure S3), which marks the maximum sedimentary age of this sample and fits well with the regional tectonics. The nephrite-forming metasomatism age at 3.3 ± 1.7 Ma, younger than the collision-starting age ~6.5 Ma (Lin *et al*. 2003), clearly demonstrates that the Fengtien nephrite formed during the arc-continent collision processes, postdating South China Sea plate subduction.

Peak metamorphic condition for HP rocks in the Yuli belt was estimated at ~550°C and 10–12 kbar (Beyssac *et al*. 2008). The temperature condition of the greenschist-facies metamorphic rocks in the southern part of the Yuli belt, supposedly related to arc-continental collision, was suggested to be around 470°C (Beyssac *et al*. 2007). The metamorphic temperature estimate for mica-quartz schist in the Fengtien area in the northern Yuli belt is around 410–430°C (Table 2, see Section 4.1). These temperature estimates, all based on the RSCM thermometry, are higher than the temperature of nephrite formation at Fengtien, which was inferred to be around 320–420°C, or even lower (see Section 4.1). Given that the mica-quartz schist was metasomatically replaced by epidote-clinozoisite and chlorite along cleavages, as well as the presence of metasomatic fissure-filling minerals within all lithologies, the formation of the Fengtien nephrite would thus have taken place during the retrograde cooling, rather than the prograde heating, stage. Prominent retrograde cooling generally resulted from rock exhumation, which was most likely triggered by arc-continent collision in the Taiwan region (e.g. Beyssac *et al*. 2007). From this temperature information, the Fengtien nephrite would thus have formed during the collision-induced metamorphism, and the related metasomatic processes might have even lasted during the subsequent cooling. This tectonic inference from temperature estimates and field/petrographic observations is in accord with the dating results. Note that the above discussion does not exclude the possibility that this specific ultramafic-country rock assemblage at Fengtien might actually have been entrained into the subduction-accretionary complex not long ago before arc-continent collision and was never subducted to great depths before exhumation.

5.2. Timing of regional metamorphism in terms of tectonic event

In the Yuli subduction-accretionary complex, large serpentinite bodies outcrop in the Fengtien, Wanjung, Juisui, and Yuli areas (Figure 1a). HP rocks, omphacite-zoisite metabasite and glaucophane schist, were only reported in association with the Wanjung and the Juisui serpentinites, respectively (Liou *et al*. 1975; Yui and Lo 1989; Beyssac *et al*. 2008). These HP rock-serpentinite associations were suggested occurring as blocks thrust on top of other Yuli rocks, mostly with greenschist-facies mineral assemblages, during the Pleistocene (Yang and Wang 1985; Lin 1999). On the other hand, the Fengtien and Yuli serpentinites were suggested as blocks scraped off of ultramafic bodies within Yuli greenschist-facies pelitic schist (Lin *et al*. 1984). The lack of convincing HP indicators in most rocks, including metabasites, in the Yuli belt has been a contentious issue for decades.

In the Fengtien serpentinite area, HP minerals were not observed. However, the formation of diopsidite, nephrite, and clinozoisite rock between serpentinite and mica-quartz schist clearly demonstrates that fluid infiltration, metasomatism, and mineral recrystallization were taking place during rock exhumation resulting from arc-continent collision as discussed previously. Following this conclusion, the observed metamorphic characteristics of the Yuli belt

can thus be explained if the HP rocks formed during subduction were later subjected to a fluid-mediated Barrovian-type metamorphic overprinting during the subsequent arc-continent collision (e.g. Maruyama *et al*. 2010). The higher geothermal gradient for this Barrovian overprint could have largely been a corollary of fast exhumation of the HP rocks to a shallow depth (i.e. isothermal decompression) triggered by arc-continent collision. The exhumation of these HP rocks might in fact have been related to the subduction of the forearc lithosphere during arc-continent collision (Froitzheim *et al*. 2003). The subducted forearc lithosphere was recently seismically imaged by Shyu *et al*. (2011). Under this circumstance, HP index minerals would have been almost completely replaced by the greenschist-facies ones during collision, most likely facilitated by rock shearing as well as by fluid infiltration sourced from the yet deeply subducted rocks underneath. Only a few HP records survived from this intensive superimposed metamorphism, as demonstrated recently by detailed chemical analyses on various Ca- and Na-amphiboles within the Juisui glaucophane schist (Tsai *et al*. 2013). Successive thrusting during rock exhumation as a result of arc-continent collision would emplace HP rocks on top of the shallow greenschist-facies rocks.

The reliable age dating data, excluding low-temperature fission track and (U-Th)/He ages, from the Yuli belt are compiled in Table 4. The dates, all derived from rocks associated with serpentinites, show three age ranges: ~79 Ma, ~11 Ma, and 5–3 Ma. The young ages, 5–3 Ma, include the inferred nephrite formation age given here, a resetting age of an epidote amphibolite severely affected by invasion of fluid-forming quartz veins (Jahn *et al*. 1981) and a cooling age of phlogopite from omphacite-zoisite metabasite (Lo and Yui 1996). These ages, equivalent within analytical errors, could be interpreted as the time of the fluid-mediated Barrovian-type arc-continent collision metamorphism and/or the subsequent cooling. These dates also suggest that all these rocks shared similar T-t paths after the collision metamorphism.

The age of ~11 Ma from glaucophane schist, on the other hand, indicates the time of HP metamorphism or subsequent cooling in response to subduction of the South China Sea plate, considering that the P-T condition of the HP rocks was ~550°C and 10–12 kbar (Beyssac *et al*. 2008), and the blocking temperature of Ar diffusion for phengite studied by Lo and Yui (1996) in Table 4 would be in the range of 430–460°C based on the recent experimental diffusion data by Harrison *et al*. (2009) under 10 kbar and a cooling rate of 10°C/Ma. However, the temperature condition for the collision-related greenschist-facies metamorphism was suggested to be around 410–470°C for the Yuli rocks according to Beyssac *et al*. (2007) and the present work (Table 2). This temperature range is high enough to reset the ^{40}Ar-^{39}Ar system in phengite of glaucophane schist to an age younger than 6.5 Ma or to disturb the age spectrum, theoretically. Both the predicted consequences, however, were not reported by Lo and Yui (1996). Discrepancy is obviously present among data sets. The temperature estimate of 410–470°C was based on the RSCM, which is a robust proxy and may not be subjected to retrograde overprinting (Beyssac *et al*. 2002). This apparent discrepancy could be reconciled if the temperature of 410–470°C on greenschist-facies rocks is interpreted as subduction-related, instead of collision-related, because the Yuli belt is a Cenozoic, rather than a Mesozoic, subduction-accretionary complex. In this respect, the HP metamorphic environment in the area might have prevailed only at depth during subduction but may actually have not been well developed in the shallow subduction zone, because the subducted South China Sea plate was young and hot (e.g. Maruyama and Okamoto 2007 and references therein). Collision-related metamorphism may have occurred at lower temperature conditions, as evidenced by the temperature estimates for nephrite formation. A schematic diagram showing the asserted tectonic evolution is thus given in Figure 7. More detailed work is necessary to delineate the T-t history of various parts of the Yuli belt.

The age of ~79 Ma for an epidote amphibolite sample from the Juisui area is based on a 4-point Rb-Sr isochron (Jahn *et al*. 1981) and has been regarded as evidence that the Yuli belt is of Cretaceous age. However, because Cenozoic detrital zircons from the Yuli belt were reported recently (Lo *et al*. 2012; Chen *et al*. 2013; Yui 2013), the Rb-Sr age becomes a enigma

Table 4. Available radiogenic isotope dating results from rocks of the Yuli belt.

Rock	Method (mineral[a])	Age (Ma)	Locality	Reference
epidote amphibolite	Rb-Sr (mineral isochron)	79 ± 7	Juisui	Jahn *et al*. (1981)
epidote amphibolite	Rb-Sr (mineral isochron)	4.6 ± 0.6	Juisui	Jahn *et al*. (1981)
glaucophane schist	Rb-Sr (whole rock/amp-ph)	8 to 14	Juisui	Jahn *et al*. (1981)
glaucophane schist	^{40}Ar-^{39}Ar (ph)	11.3 ± 0.1	Juisui	Lo and Yui (1996)
omphacite-zoisite metabasite	^{40}Ar-^{39}Ar (phl)	4.4 ± 0.1	Wanjung	Lo and Yui (1996)
clinozoisite rock	U-Pb (zrn rim)	3.3 ± 1.7	Fengtien	This study

Note: [a]Mineral abbreviation: amp, amphibole; ph, phengite; phl, phlogopite; zrn, zircon.

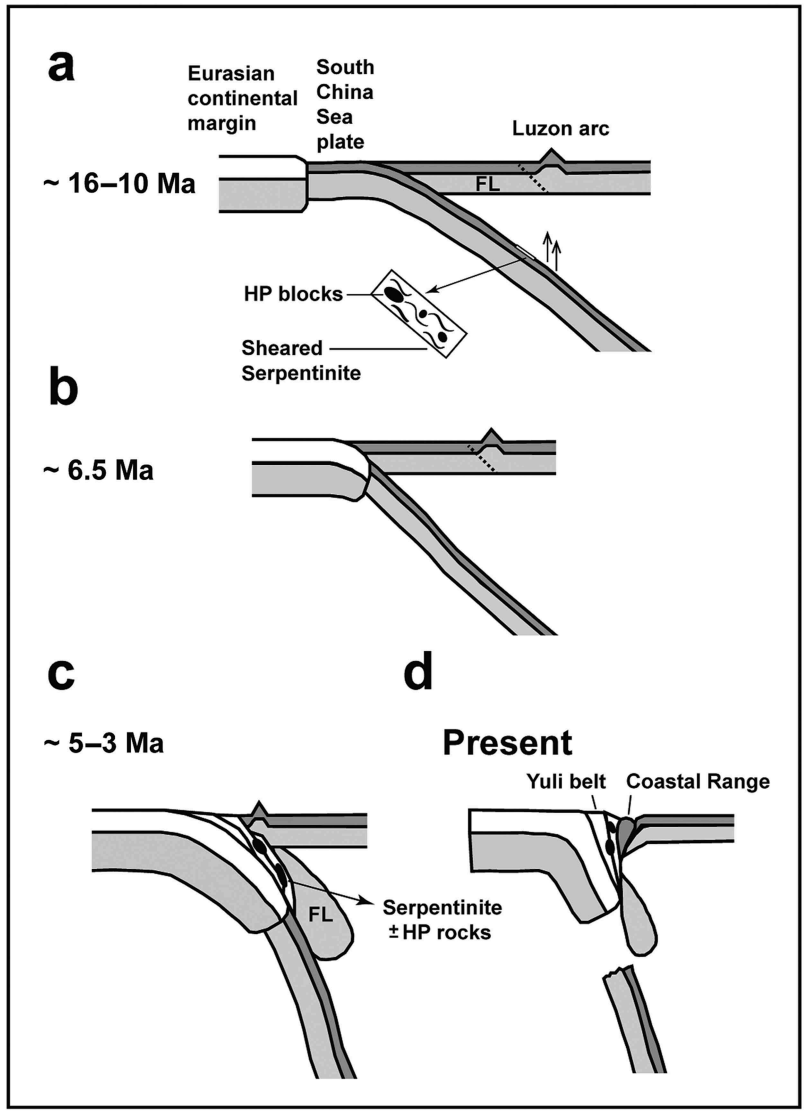

Figure 7. Schematic diagram (not in scale) depicting the tectonics of the area since the middle Miocene. (a) At ~16–10 Ma, young and hot South China Sea plate subducted eastward forming the Luzon arc. HP metamorphism took place only at depths. Subducting serpentinite mélange including HP blocks occurred at the plate interface. (b) At ~6.5 Ma, the Luzon arc (and the forearc lithosphere) began to collide with the Eurasian plate margin. (c) At ~5–3 Ma, the subducted Yuli (HP) rocks exhumed to a shallower depth triggered by arc-continent collision and was subjected to a fluid-mediated Barrovian-type metamorphic overprint. The forearc lithosphere (FL) underthrusted eastward as imaged by seismic tomography (Shyu *et al*. 2011). Nephrite was formed during this period of time. (d) At present, the Yuli belt exhumes at the surface and the northern part of the Luzon arc (i.e. the Coastal Range) is accreting to the continental margin.

since both the South China Sea plate (37–15 Ma; Hsu *et al*. 2004) and the West Philippine Sea plate (55–33/30 Ma; Deschamps and Lallemand 2002) are of Cenozoic age. We tentatively interpret this as indicating an exogenous block incorporated during subduction or exhumation from a Late Cretaceous shear zone of the overlying Huatung microplate. This microplate is of Cretaceous age and located west of the Gagua Ridge (Figure 1a, inset) and would be the base of the northern Luzon arc (Deschamps *et al*. 2000).

6. Concluding remarks

Harlow and Sorensen (2005) and Harlow *et al*. (2007, 2014) compiled nephrite occurrences associated with 'serpentinite mélange' or 'ophiolitic serpentinite' within subduction-accretionary complexes around the world. Although detailed information for most of the nephrite occurrences is not available, common features include (1) contemporaneous (tectonic) stress during metasomatic processes is essential in forming nephrite; (2) the P-T conditions for nephrite formation would be low, although

Table 5. Major nephrite deposits associated with serpentinite around the world.

Locality	Age of sediments	Metamorphic age	Nephrite age (method)	References
East Sayan, Siberia, Russia	Neoproterozoic(?)	~800 Ma	?	Prokhor (1991); Kuzmichev *et al*. (2007); Kuzmichev and Larionov (2013)
Alaska, USA	Devonian-Jurassic	Jurassic-Cretaceous	?	Till *et al*. (2008) and the references therein
British Columbia, Canada	Late Palaeozoic-Triassic	Jurassic-Cretaceous	?	Leaming (1978)
South Island, New Zealand	Permian-Triassic	240–250, 190–210, 150–120, and 5–10 Ma	>6 Ma (?) (Rb-Sr, tremolite)	Adams *et al*. (2007) and the references therein
Tamworth, South Australia	Silurian-Devonian	Permian	273–280 Ma ($^{40}Ar/^{39}Ar$ tremolite)	Lanphere and Hockley (1976); Hockley *et al*. (1978)
Fengtien, Taiwan	Miocene	Miocene-Pliocene	3.3 ± 1.7 Ma (U-Pb zircon)	This study

difficult to constrain quantitatively; and (3) the country rocks mainly contain prehnite-pumpellyite facies to greenschist-facies mineral assemblages, and HP minerals are seldom present nearby or were mostly replaced by low-grade ones. With all these common characteristics, the formation of Fengtien nephrite within the framework of regional tectonics may serve as a working model for future studies on other nephrite occurrences.

The temporal information, including the ages of sedimentation and metamorphism of the country rocks, as well as the time of nephrite formation, of some major nephrite deposits around the world is given in Table 5. Although the nephrite formation age, in most cases, is not known, the hosting subduction-accretionary complexes mostly are of Mesozoic age or even older. In this respect, the Fengtien nephrite would be the youngest one of its kind now exposed on Earth's surface.

Lastly, it may be worth mentioning that although dating zircon rims with a thickness of ~20–50 μm from high-grade metamorphic rocks or high-temperature hydrothermal veins by ion or laser probe instruments (SIMS and LA-ICPMS) has become increasingly common in the past decades (see Ireland and Williams 2003; Košler and Sylvester 2003), the present work, to the authors' knowledge, would be the first U-Pb dating case on low-temperature hydrothermal thin (<15–20 μm) zircon rim by NanoSIMS. Future applications can be expected.

Acknowledgements

Helpful suggestions and comments from R.J. Stern, G.E. Harlow, and T. Tsujimori are highly appreciated.

Funding

This study was financially supported by the Ministry of Science and Technology, Taiwan [grant number NSC 101-2116-M-001-004-MY3].

Supplemental data

Supplemental data for this article can be accessed http://dx.doi.org/10.1080/00206814.2014.972994

References

Adams, C.J., Beck, R.J., and Campbell, H.J., 2007, Characterisation and origin of New Zealand nephrite jade using its strontium isotopic signature: Lithos, v. 97, p. 307–322. doi:10.1016/j.lithos.2007.01.001

Beyssac, O., Goffé, B., Chopin, C., and Rouzaud, J.N., 2002, Raman spectra of carbonaceous material in metasediments: A new geothermometer: Journal of Metamorphic Geology, v. 20, p. 859–871. doi:10.1046/j.1525-1314.2002.00408.x

Beyssac, O., Goffé, B., Petitet, J.-P., Froigneux, E., Moreau, M., and Rouzaud, J.-N., 2003, On the characterization of disordered and heterogeneous carbonaceous materials by Raman spectroscopy: Spectrochimica Acta Part A: Molecular and Biomolecular Spectroscopy, v. 59, p. 2267–2276. doi:10.1016/S1386-1425(03)00070-2

Beyssac, O., Negro, F., Simoes, M., Chan, Y.C., and Chen, Y.G., 2008, High-pressure metamorphism in Taiwan: From oceanic subduction to arc-continent collision?: Terra Nova, v. 20, p. 118–125. doi:10.1111/j.1365-3121.2008.00796.x

Beyssac, O., Simoes, M., Avouac, J.P., Farley, K.A., Chen, Y.-G., Chan, Y.-C., and Goffé, B., 2007, Late Cenozoic metamorphic evolution and exhumation of Taiwan: Tectonics, v. 26, p. TC6001. doi:10.1029/2006TC002064

Bulle, F., Bröcker, M., Gärtner, C., and Keasling, A., 2010, Geochemistry and geochronology of HP mélanges from Tinos and Andros, Cycladic blueschist belt, Greece: Lithos, v. 117, p. 61–81. doi:10.1016/j.lithos.2010.02.004

Chen, W.S., Chung, S.L., and Shao, W.Y., 2013, U-Pb dating on detrital zircons from Yuli belt, Tananao Schist: 2013 Taiwan Geosciences Assembly, Taoyuang, Taiwan, Abstract, V3-3B-07.

Deschamps, A., and Lallemand, S., 2002, The West Philippine Basin: An Eocene to early Oligocene back arc basin opened between two opposed subduction zones: Journal of Geophysical Research, v. 107, p. 2322. doi:10.1029/2001JB001706

Deschamps, A., Monié, P., Lallemand, S., Hsu, S.K., and Yeh, K.Y., 2000, Evidence for Early Cretaceous oceanic crust trapped in the Philippine Sea plate: Earth and Planetary Science Letters, v. 179, p. 503–516. doi:10.1016/S0012-821X(00)00136-9

Flores, K.E., Martens, U.C., Harlow, G.E., Brueckner, H.K., and Pearson, N.J., 2013, Jadeitite formed during subduction: In situ zircon geochronology constraints from two different tectonic events within the Guatemala suture zone: Earth and Planetary Science Letters, v. 371–372, p. 67–81. doi:10.1016/j.epsl.2013.04.015

Froitzheim, N., Pleuger, J., Roller, S., and Nagel, T., 2003, Exhumation of high- and ultrahigh-pressure metamorphic rocks by slab extraction: Geology, v. 31, p. 925–928. doi:10.1130/G19748.1

Harlow, G.E., and Sorensen, S.S., 2005, Jade (nephrite and jadeitite) and serpentinite: Metasomatic connections: International Geology Review, v. 47, p. 113–146. doi:10.2747/0020-6814.47.2.113

Harlow, G.E., Sorensen, S.S., and Sisson, V.B., 2007, Jade, *in* Groat, L.A., ed., The geology of gem deposits: Short course handbook series, Volume 37: Quebec, Mineralogical Association of Canada, p. 207–254.

Harlow, G.E., Sorensen, S.S., Sisson, V.B., and Shi, G., 2014, The Geology of jade deposits, *in* Groat, L.A., ed., The geology of gem deposits (Second edition): Short course handbook series, Volume 44: Quebec, Mineralogical Association of Canada, p. 305–374.

Harrison, T.M., Célérier, J., Aikman, A.B., Hermann, J., and Heizler, M.T., 2009, Diffusion of ^{40}Ar in muscovite: Geochimica et Cosmochimica Acta, v. 73, p. 1039–1051. doi:10.1016/j.gca.2008.09.038

Ho, C.S., 1986, An introduction to the geology of Taiwan: Explanatory text of the Geologic Map of Taiwan: R.O.C, Ministry of Economic Affairs, 163 p.

Hockley, J.J., Birch, W.D., and Worner, H.K., 1978, A nephrite deposit in the great serpentine belt of New South Wales: Journal of the Geological Society of Australia, v. 25, p. 249–254. doi:10.1080/00167617808729033

Hsu, S.-K., Yeh, Y., Doo, W.-B., and Tsai, C.-H., 2004, New bathymetry and magnetic lineations identifications in the northernmost South China Sea and their tectonic implications: Marine Geophysical Researches, v. 25, p. 29–44. doi:10.1007/s11001-005-0731-7

Ireland, T.R., and Williams, I.S., 2003, Considerations in zircon geochronology by SIMS, *in* Hanchar, J.M., and Hoskin, P.W.O., eds., Zircon: Reviews in mineralogy and geochemistry, Volume 53: Mineralogical Society of America, p. 243–275.

Jahn, B.M., Liou, J.G., and Nagasawa, H., 1981, High-pressure metamorphic rocks of Taiwan – REE geochemistry, Rb-Sr ages and tectonic implications: Memoir of the Geological Society of China, v. 4, p. 497–520.

Jahn, B.M., Martineau, F., Peucat, J.J., and Cornichet, J., 1986, Geochronology of the Tananao schist complex, Taiwan, and its regional tectonic significance: Tectonophysics, v. 125, p. 103–124. doi:10.1016/0040-1951(86)90009-0

Košler, J., and Sylvester, P.J., 2003, Present trends and the future of zircon in geochronology: Laser ablation ICPMS, *in* Hanchar, J.M., and Hoskin, P.W.O., eds., Zircon: Reviews in mineralogy and geochemistry, Volume 53: Mineralogical Society of America, p. 215–241.

Kuzmichev, A., Sklyarov, E., Postnikov, A., and Bibikova, E., 2007, The Oka Belt (Southern Siberia and Northern Mongolia): A Neoproterozoic analog of the Japanese Shimanto Belt?: Island Arc, v. 16, p. 224–242. doi:10.1111/j.1440-1738.2007.00568.x

Kuzmichev, A.B., and Larionov, A.N., 2013, Neoproterozoic island arcs in East Sayan: Duration of magmatism (from U–Pb zircon dating of volcanic clastics): Russian Geology and Geophysics, v. 54, p. 34–43. doi:10.1016/j.rgg.2012.12.003

Lanari, P., Wagner, T., and Vidal, O., 2014, A thermodynamic model for di-trioctahedral chlorite from experimental and natural data in the system MgO-FeO-Al_2O_3-SiO_2-H_2O: Applications to P-T sections and geothermometry: Contributions to Mineralogy and Petrology, v. 167, p. 967–985. doi:10.1007/s00410-014-0968-8

Lanphere, M.A., and Hockley, J.J., 1976, The age of nephrite occurrences in the great serpentine belt of New South Wales: Journal of the Geological Society of Australia, v. 23, p. 15–17. doi:10.1080/00167617608728918

Leaming, S.F., 1978, Jade in Canada: Geological Survey of Canada Papers, v. 78–19, p. 1–59.

Lin, A.T., Watts, A.B., and Hesselbo, S.P., 2003, Cenozoic stratigraphy and subsidence history of the South China Sea margin in the Taiwan region: Basin Research, v. 15, p. 453–478. doi:10.1046/j.1365-2117.2003.00215.x

Lin, M.L., 1999, Litho-stratigraphy and structural geology of Wanjung area, eastern Taiwan and their implications: Journal of Geological Society of China, v. 42, p. 247–267.

Lin, M.L., Yang, C.N., and Wang, Y., 1984, Petrotectonic study on the Yuli belt of the Tananao schist in the Chinshuichi area, eastern Taiwan: Acta Geologica Taiwanica, v. 22, p. 151–188.

Liou, J.G., Ho, C.O., and Yen, T.P., 1975, Petrology of some Glaucophane schist and related rocks from Taiwan: Journal of Petrology, v. 16, p. 80–109. doi:10.1093/petrology/16.1.80

Lo, C.H., and Yui, T.F., 1996, ^{40}Ar/^{39}Ar dating of high-pressure rocks in the Tananao basement complex, Taiwan: Journal of Geological Society of China, v. 39, p. 13–130.

Lo, Y.J., Lo, C.H., and Lee, Y.H., 2012, Miocene event in Yuli belt, Tananao metamorphic complex: Annual meeting of Geological Society at Taipei, Chungli, Taiwan, Abstract, p. 238.

Maruyama, S., Masago, H., Katayama, I., Iwase, Y., Toriumi, M., Omori, S., and Aoki, K., 2010, A new perspective on metamorphism and metamorphic belts: Gondwana Research, v. 18, p. 106–137. doi:10.1016/j.gr.2010.03.007

Maruyama, S., and Okamoto, K., 2007, Water transportation from the subducting slab into the mantle transition zone: Gondwana Research, v. 11, p. 148–165. doi:10.1016/j.gr.2006.06.001

Paces, J.B., and Miller Jr., J.D., 1993, Precise U-Pb ages of Duluth Complex and related mafic intrusions, northeastern Minnesota: Geochronological insights to physical, petrogenetic, paleomagnetic, and tectonomagmatic processes associated with the 1.1 Ga Midcontinent Rift System: Journal of Geophysical Research, v. 98, p. 13997–14013. doi:10.1029/93JB01159

Prokhor, S.A., 1991, The genesis of nephrite and emplacement of the nephrite-bearing ultramafic complexes of East Sayan: International Geology Review, v. 33, p. 290–300. doi:10.1080/00206819109465694

Schmitz, M.D., Bowring, S.A., and Ireland, T.R., 2003, Evaluation of Duluth Complex anorthositic series (AS3) zircon as a U-Pb geochronological standard: New high-precision isotope dilution thermal ionization mass spectrometry results: Geochimica Et Cosmochimica Acta, v. 67, p. 3665–3672. doi:10.1016/S0016-7037(03)00200-X

Shyu, J.B.H., Wu, Y.-M., Chang, C.-H., and Huang, -H.-H., 2011, Tectonic erosion and the removal of forearc lithosphere during arc-continent collision: Evidence from

recent earthquake sequences and tomography results in eastern Taiwan: Journal of Asian Earth Sciences, v. 42, p. 415–422. doi:10.1016/j.jseaes.2011.05.015

Stacey, J.S., and Kramers, J.D., 1975, Approximation of terrestrial lead isotope evolution by a two-stage model: Earth and Planetary Science Letters, v. 26, p. 207–221. doi:10.1016/0012-821X(75)90088-6

Stern, R.J., Tsujimori, T., Harlow, G.E., and Groat, L., 2013, Plate Tectonic Gemstones: Geology, v. 41, p. 723–726. doi:10.1130/G34204.1

Takahata, N., Tsutsumi, Y., and Sano, Y., 2008, Ion microprobe U–Pb dating of zircon with a 15 micrometer spatial resolution using NanoSIMS: Gondwana Research, v. 14, p. 587–596. doi:10.1016/j.gr.2008.01.007

Tan, L.P., Wang Lee, C., Chen, C.C., Tien, P.L., Tsui, P.C., and Yui, T.F., 1978, A mineralogical study of the Fengtien nephrite deposits of Hualien: Taiwan, National Science Council Special Publication, no. 1, 81 p.

Till, A.B., Dumoulin, J.A., Harris, A.G., Moore, T.E., Bleick, H. A., and Siwiec, B.R., 2008, Bedrock geologic map of the southern Brooks Range, Alaska, and accompanying conodont data: U.S. Geological Survey, Open-File Report 2008-1149, 88 p.

Tsai, C.H., Iizuka, Y., and Ernst, W.G., 2013, Diverse mineral compositions, textures, and metamorphic P–T conditions of the glaucophane-bearing rocks in the Tamayen mélange, Yuli belt, eastern Taiwan: Journal of Asian Earth Sciences, v. 63, p. 218–233. doi:10.1016/j.jseaes.2012.09.019

Tsai, Y.-B., 1986, Seismotectonics of Taiwan: Tectonophysics, v. 125, p. 17–37. doi:10.1016/0040-1951(86)90005-3

Tsujimori, T., and Harlow, G.E., 2012, Petrogenetic relationships between jadeitite and associated high-pressure and low-temperature metamorphic rocks in worldwide jadeitite localities: A review: European Journal of Mineralogy, v. 24, p. 371–390. doi:10.1127/0935-1221/2012/0024-2193

Yang, C.N., and Wang, Y., 1985, Petrotectonic study on the Yuli belt of the Tananao Schist in the Juisui area, eastern Taiwan: Acta Geologica Taiwanica, v. 23, p. 149–176.

Yang, T.F., Tien, J.-L., Chen, C.-H., Lee, T., and Punongbayan, R.S., 1995, Fission-track dating of volcanics in the northern part of the Taiwan-Luzon Arc: Eruption ages and evidence for crustal contamination: Journal of Southeast Asian Earth Sciences, v. 11, p. 81–93. doi:10.1016/0743-9547(94)00041-C

York, D., 1968, Least squares fitting of a straight line with correlated errors: Earth and Planetary Science Letters, v. 5, p. 320–324. doi:10.1016/S0012-821X(68)80059-7

Yui, T.F., 2013, The Tananao metamorphic basement of Taiwan: A revisit: Tectonics of Taiwan: An International Conference (TOTIC), Taoyuan, Taiwan, Abstract, U5-5A-06.

Yui, T.-F., Fukoyama, M., Iizuka, Y., Wu, C.-M., Wu, T.-W., Liou, J.G., and Grove, M., 2013, Is Myanmar jadeitite of Jurassic age? A result from incompletely recrystallized inherited zircon: Lithos, v. 160–161, p. 268–282. doi:10.1016/j.lithos.2012.12.011

Yui, T.-F., Heaman, L., and Lan, C.-Y., 1996, U-Pb and Sr isotopic studies on granitoids from Taiwan and Chinmen-Lieyü and tectonic implications: Tectonophysics, v. 263, p. 61–76. doi:10.1016/S0040-1951(96)00023-6

Yui, T.F., and Lo, C.H., 1989, High-pressure metamorphosed ophiolitic rocks from the Wanjung area, Taiwan: Proceedings of the Geological Society of China, v. 32, p. 47–62.

Yui, T.F., Maki, K., Lan, C.Y., Hirata, T., Chu, H.T., Kon, Y., Yokoyama, T.D., Jahn, B.M., and Ernst, W.G., 2012, Detrital zircons from the Tananao metamorphic complex of Taiwan: Implications for sediment provenance and Mesozoic tectonics: Tectonophysics, v. 541–543, p. 31–42. doi:10.1016/j.tecto.2012.03.013

Yui, T.-F., Maki, K., Usuki, T., Lan, C.-Y., Martens, U., Wu, C.-M., Wu, T.-W., and Liou, J.G., 2010, Genesis of Guatemala jadeitite and related fluid characteristics: Insight from zircon: Chemical Geology, v. 270, p. 45–55. doi:10.1016/j.chemgeo.2009.11.004

Yui, T.F., Okamoto, K., Usuki, T., Lan, C.Y., Chu, H.T., and Liou, J.G., 2009, Late Triassic–Late Cretaceous accretion/subduction in the Taiwan region along the eastern margin of South China – evidence from zircon SHRIMP dating: International Geology Review, v. 51, p. 304–328. doi:10.1080/00206810802636369

Yui, T.F., and Wang Lee, C., 1980, Metasomatism of ultramafic rocks from Laonaoshan, eastern slope of the Central Range, Taiwan: Proceedings of the Geological Society of China, v. 23, p. 92–104.

Yui, T.-F., Yeh, H.-W., and Wang Lee, C., 1988, Stable isotope studies of nephrite deposits from Fengtien, Taiwan: Geochimica et Cosmochimica Acta, v. 52, p. 593–602. doi:10.1016/0016-7037(88)90321-3

Yui, T.-F., Yeh, H.-W., and Wang Lee, C., 1990, A stable isotope study of serpentinization in the Fengtien ophiolite, Taiwan: Geochimica Et Cosmochimica Acta, v. 54, p. 1417–1426. doi:10.1016/0016-7037(90)90165-H

Zane, A., Sassi, R., and Guidotti, C.V., 1998, New data on metamorphic chlorite as a petrogenetic indicator mineral, with special regard to greenschist-facies rocks: Canadian Mineralogists, v. 36, p. 713–726.